High-pressure Synthesis and Characterization of the Rare-earth Fluoride Borate LaB_2O_4F

Ernst Hinteregger[a], Krisztina Kocsis[a], Thomas S. Hofer[a], Gunter Heymann[a], Lukas Perfler[b], and Hubert Huppertz[a]

[a] Institut für Allgemeine, Anorganische und Theoretische Chemie, Leopold-Franzens-Universität Innsbruck, Innrain 80–82, A-6020 Innsbruck, Austria

[b] Institut für Mineralogie und Petrographie, Leopold-Franzens-Universität Innsbruck, Innrain 52f, A-6020 Innsbruck, Austria

Reprint requests to H. Huppertz. E-mail: Hubert.Huppertz@uibk.ac.at

Z. Naturforsch. **2013**, *68b*, 951 – 959 / DOI: 10.5560/ZNB.2013-3177
Received June 24, 2013

The rare-earth fluoride borate LaB_2O_4F was synthesized under high-pressure/high-temperature conditions of 1.1 GPa and 1300 °C in a Walker-type multianvil apparatus from lanthanum oxide, lanthanum fluoride, and boron oxide. The single-crystal structure determination revealed that LaB_2O_4F is isotypic to CeB_2O_4F. The compound crystallizes in the orthorhombic space group *Pbca* (no. 61) with eight formula units and the lattice parameters $a = 8.2493(9)$, $b = 12.6464(6)$, $c = 7.3301(5)$ Å, $V = 764.7(2)$ Å^3, $R_1 = 0.0354$, and $wR_2 = 0.0474$ (all data). The structure exhibits a 9+1 coordinated lanthanum cation, one threefold coordinated fluoride ion and a chain of corner-sharing $[BO_3]^{3-}$ groups. In addition to the IR- and Raman-spectroscopic investigations, DFT calculations were performed to support the assignment of the vibrational bands.

Key words: High Pressure, Borate, Crystal Structure, DFT

Introduction

In the past, our research using the multianvil high-pressure technique provided us with a variety of new borates with fascinating structures [1]. More recently we extended our interests into the field of rare-earth fluoride and fluorido borates. The difference between these two classes of compounds concerns the different chemical bonding situation of the fluorine atoms. Fluoride borates possess fluoride anions while in fluorido borates the fluorine atoms are covalently bonded to a boron atom (old designation: fluoroborate). Interestingly, no fluorido borate could be synthesized under high-pressure conditions up to now. Due to the high flexibility of the BO_3 and BO_4 groups to form structures with isolated BO_3 and BO_4 groups, discrete groups (*e. g.* $[B_3O_6]^{3-}$), chains, layers, or complicated networks *via* the linkage of the corners of the groups or *via* edge-sharing of BO_4 tetrahedra, it is more than likely that a large number of new compounds with interesting properties can be expected in the future. At the beginning of our research in the field of fluoride borates, the system *RE*-B-O-F was only represented by the rare-earth fluoride borates $RE_3(BO_3)_2F_3$(*RE* = Sm, Eu, Gd) [2, 3] and $Gd_2(BO_3)F_3$ [4]. These compounds were synthesized under ambient-pressure conditions by heating stoichiometric mixtures of RE_2O_3, B_2O_3 and REF_3. A closer look into the class of rare-earth fluoride borates shows various compounds for the rare-earth cations Pr^{3+}–Nd^{3+} and Sm^{3+}–Yb^{3+}. In contrast, the rare-earth cations La^{3+} and Ce^{3+} are represented in each case by only a single compound namely $La_4B_4O_{11}F_2$ [5] and CeB_2O_4F [6], respectively. In fact, a lutetium fluoride borate is unknown up to now. For this reason, we focused our research on rare-earth fluoride borates with the cations La^{3+}, Ce^{3+}, and Lu^{3+}. In this work, we report on the high-pressure/high-temperature synthesis of LaB_2O_4F, wherewith we discovered the first isotypic compound of the recently published cerium fluoride borate CeB_2O_4F [6]. Because of the relatively mild pressure conditions, all boron atoms of the compound LaB_2O_4F are coordinated by three oxygen atoms, forming trigonal-planar $[BO_3]^{3-}$ groups, which

© 2013 Verlag der Zeitschrift für Naturforschung, Tübingen · http://znaturforsch.com

are connected to chains. In the following, we describe the synthesis, the single-crystal structure determination, and Raman-, and IR-spectroscopic investigations of LaB_2O_4F as well as quantum-chemical calculations of harmonic vibrational frequencies.

Experimental Section

Synthesis

The new lanthanum fluoride borate LaB_2O_4F was synthesized from a stoichiometric mixture of La_2O_3, B_2O_3, and LaF_3 (all chemicals from Strem Chemicals, Newburyport, USA 99.9+%) according to Eq. 1.

$$La_2O_3 + 3\ B_2O_3 + LaF_3 \xrightarrow{1.1\ \text{GPa},\ 1300\,^\circ\text{C}} 3\ LaB_2O_4F \quad (1)$$

The starting materials were finely ground and filled into a boron nitride crucible (Henze BNP GmbH, HeBoSint® S100, Kempten, Germany). The boron nitride crucible was placed into an 18/11-assembly and compressed by eight tungsten carbide cubes (TSM-10, Ceratizit, Reutte, Austria). To apply the pressure, a 1000 t multianvil press with a Walker-type module (both devices from the company Voggenreiter, Mainleus, Germany) was used. A detailed description of the assembly preparation can be found in refs. [7–11]. In detail, the 18/11 assembly was compressed up to 1.1 GPa in 35 min and heated to 1300 °C (cylindrical graphite furnace) in the following 10 min, kept there for 8 min and cooled down to 450 °C in 20 min at constant pressure. After natural cooling down to room temperature by switching off the heating, a decompression period of two hours was required. The recovered MgO octahedron (pressure transmitting medium, Ceramic Substrates & Components Ltd., Newport, Isle of Wight, UK) was broken apart, and the sample was carefully separated from the surrounding graphite and boron nitride crucible. The new compound LaB_2O_4F was gained in the form of colorless, air- and water-resistant crystals.

All efforts to synthesize LaB_2O_4F under ambient pressure conditions were in vain. The high-temperature syntheses were performed in boron nitride crucibles (Henze BNP GmbH, HeBoSint® S100, Kempten, Germany) which were placed into silica glass tubes. These assemblies were heated under ambient pressure conditions in a tube furnace from the company Carbolite.

Crystal structure analysis

The powder diffraction pattern was obtained in transmission geometry, using a Stoe Stadi P powder diffractometer with Ge(111)-monochromatized Mo$K_{\alpha 1}$ ($\lambda = 70.93$ pm) radiation. Fig. 1 shows the experimental powder pattern of LaB_2O_4F that matches well with the theoretical pattern simulated from the single-crystal data. Small single crystals of LaB_2O_4F were isolated by mechanical fragmentation. The single-crystal intensity data were collected at room temperature using a Nonius Kappa-CCD diffractometer with graphite-monochromatized MoK_α radiation ($\lambda = 71.073$ pm). A semiempirical absorption correction based on equivalent and redundant intensities (SCALEPACK [12]) was applied to the intensity data. All relevant details of the data collection and evaluation are listed in Table 1. According to the systematic extinctions, the orthorhombic space group *Pbca* was derived. Due to the fact that LaB_2O_4F is isotypic to CeB_2O_4F [6], the structural

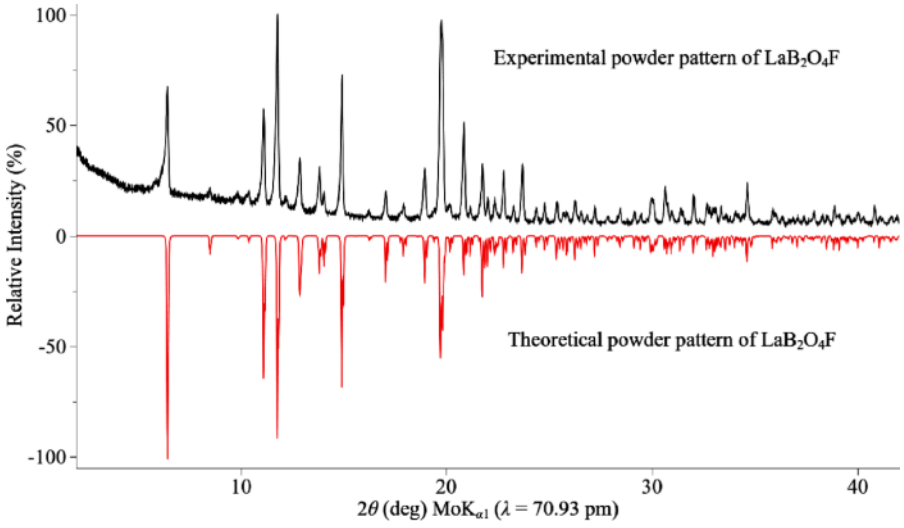

Fig. 1 (color online). Experimental powder pattern (top) of LaB_2O_4F, compared with the theoretical powder pattern (bottom) simulated from single-crystal data.

Table 1. Crystal data and structure refinement of LaB_2O_4F (space group: *Pbca*) with standard deviations in parentheses where available.

Empirical formula	LaB_2O_4F
Molar mass, g·mol^{-1}	243.53
Crystal system	orthorhombic
Space group	*Pbca* (no. 61)
Lattice parameters from powder data	
Powder diffractometer	Stoe Stadi P
Radiation	Mo$K_{\alpha1}$ ($\lambda = 70.93$ pm)
a, Å	8.2483(7)
b, Å	12.6466(8)
c, Å	7.330(2)
V, Å^3	764.6(2)
Single crystal data	
Single crystal diffractometer	Enraf-Nonius Kappa CCD
Radiation	MoK_α ($\lambda = 71.073$ pm) (graded multilayer X-ray)
Crystal size, mm^3	$0.007 \times 0.004 \times 0.003$
a, Å	8.2493(9)
b, Å	12.6464(6)
c, Å	7.3301(5)
V, Å^3	764.7(2)
Formula units per cell	8
Calculated density, g·cm^{-3}	4.23
Temperature, *K*	293(2)
Absorption coefficient, mm^{-1}	11.1
F(000), e	864
θrange, deg	3.2–30.0
Range in *hkl*	$\pm11, \pm17, \pm10$
Total no. of reflections	8136
Independent reflections / R_{int}	1119 / 0.0410
Reflections with $I > 2\,\sigma(I)$ / R_σ	952 / 0.0198
Data / ref. parameters	1194 / 74
Absorption correction	multi-scan (SCALEPACK [12])
Goodness-of-fit on F_i^2	1.196
Final R_1 / wR_2 [$I > 2\,\sigma(I)$]	0.0268 / 0.0474
R_1 / wR_2 (all data)	0.0354 / 0.0499
Largest diff. peak / hole, e·Å^{-3}	1.27 / –0.65

Table 2. Atomic coordinates and equivalent isotropic displacement parameters U_{eq} (Å^2) of LaB_2O_4F (space group: *Pbca*). All atoms are positioned on the Wyckoff site 8*c*. U_{eq} is defined as one third of the trace of the orthogonalized U_{ij} tensor (standard deviations in parentheses).

Atom	*x*	*y*	*z*	U_{eq}
La1	0.11384(2)	0.47658(2)	0.25238(3)	0.00624(9)
F1	0.1342(3)	0.0491(2)	0.4312(3)	0.0127(5)
B1	0.1593(5)	0.1723(3)	0.1544(6)	0.0078(8)
B2	0.4104(5)	0.2711(3)	0.2383(6)	0.0088(7)
O1	0.1029(3)	0.0859(2)	0.0746(4)	0.0100(5)
O2	0.3263(3)	0.1792(2)	0.1912(4)	0.0113(5)
O3	0.0707(3)	0.2595(2)	0.2074(4)	0.0138(6)
O4	0.3573(3)	0.3696(2)	0.2266(4)	0.0119(6)

Table 3. Anisotropic displacement parameters (U_{ij} in Å^2) for LaB_2O_4F (space group: *Pbca*).

Atom	U_{11}	U_{22}	U_{33}	U_{23}	U_{13}	U_{12}
La1	0.0060(2)	0.0068(2)	0.0059(2)	0.00023(9)	−0.00009(8)	0.00043(6)
F1	0.014(2)	0.016(2)	0.008(2)	−0.001(2)	−0.0008(8)	0.0001(8)
B1	0.009(2)	0.006(2)	0.009(2)	0.003(2)	0.003(2)	0.001(2)
B2	0.005(2)	0.008(2)	0.014(2)	0.002(2)	0.000(2)	−0.001(2)
O1	0.013(2)	0.008(2)	0.009(2)	−0.002(2)	0.002(2)	−0.003(2)
O2	0.006(2)	0.008(2)	0.020(2)	−0.002(2)	−0.002(2)	−0.001(2)
O3	0.006(2)	0.008(2)	0.028(2)	−0.003(2)	0.004 (2)	0.000(2)
O4	0.008(2)	0.008(2)	0.019(2)	0.000(2)	0.000(2)	0.0008(9)

La1–F1a	238.2(2)	B1–O1	132.3(5)	F1– La1a	238.2(2)
La1–O4a	242.9(3)	B1–O3	137.9(5)	F1– La1b	261.5(2)
La1–O1a	249.2(3)	B1–O2	140.7(5)	F1– La1c	262.3(2)
La1–O4b	251.7(3)		Ø = 137.0		Ø = 254.0
La1–O1b	259.2(3)				
La1–F1b	261.5(2)	B2–O4	132.2(5)		
La1–F1c	262.3(2)	B2–O3	138.8(5)		
La1–O2	264.8(3)	B2–O2	139.7(5)		
La1–O3	278.8(3)		Ø = 136.9		
La1–O1c	301.2(3)				
	Ø = 261.0				

Table 4. Interatomic distances (pm) in LaB_2O_4F (space group: *Pbca*) calculated with the single-crystal lattice parameters.

O1–B1–O3	126.7(4)	O4–B2–O3	115.7(3)	La1a–F1–La1b	113.94(9)
O1–B1–O2	118.7(3)	O4–B2–O2	127.1(3)	La1a–F1–La1c	120.14(9)
O3–B1–O2	114.6(3)	O3–B1–O2	117.1(3)	La1b–F1–La1c	103.91(8)
	Ø = 120.0		Ø = 119.9		Ø = 112.7

Table 5. Interatomic angles (deg) in LaB_2O_4F (space group: *Pbca*), calculated with the single-crystal lattice parameters.

refinement was performed by taking the positional parameters of CeB_2O_4F as starting values [SHELXL-97 [13, 14] (full-matrix least-squares on F^2)]. All atoms were refined with anisotropic displacement parameters. The final difference Fourier syntheses did not reveal any significant peaks in the refinement. Tables 2–5 list the positional parameters, anisotropic displacement parameters, and interatomic distances.

Further details of the crystal structure investigation may be obtained from the Fachinformationszentrum Karlsruhe, D-76344 Eggenstein-Leopoldshafen, Germany (fax: +49-7247-808-666; E-mail: crysdata@fiz-karlsruhe.de, http://www.fiz-informationsdienste.de/en/DB/icsd/depot_anforderung.html) on quoting the deposition number CSD-426339.

Vibrational spectra

The FTIR-ATR (*A*ttenuated *T*otal *R*eflection) spectra of powders were measured with a Bruker Alpha-P spectrometer with a diamond ATR crystal ($2 \times 2\,mm^2$), equipped with a DTGS detector in the spectral range of $400-4000\,cm^{-1}$ (spectral resolution $4\,cm^{-1}$). 24 scans of the sample were acquired. A correction for atmospheric influences using the Opus 7.0 software was performed.

The single-crystal Raman spectra of LaB_2O_4F were measured in the spectral range of $50-4000\,cm^{-1}$ with a Raman micro-spectrometer LabRAM HR-800 (HORIBA Jobin Yvon GmbH, Bensheim, Germany) and hundredfold magnification. The samples were excited using the 532 nm emission line of a frequency-doubled 100 mW Nd:YAG laser and the 633 nm mission line of a 17 mW helium neon laser under an Olympus 50 × objective lens. The size of the laser spot on the surface was approximately 1 μm. The scattered light was dispersed by an optical grating with 1800 lines mm^{-1} and collected by a 1024×256 open electrode CCD detector. The spectral resolution determined by measuring the Rayleigh line was less than $2\,cm^{-1}$. The spectra were recorded unpolarized. The accuracy of the Raman line shifts, calibrated by regularly measuring the Rayleigh line, was in the order of $0.5\,cm^{-1}$. Background and Raman bands were fitted by the built-in spectrometer software LabSpec to second order polynomial and convoluted Gaussian-Lorentzian functions, respectively.

DFT calculations

In addition to the experimentally recorded IR spectrum, quantum-chemical computations of harmonic vibrational frequencies were performed using the CRYSTAL09 program [15–17]. An important step of a quantum-mechanical calculation of frequencies is the choice of adequate basis sets. A compromise has to be found balancing computational effort and accuracy of the results. To reduce the computational effort, a basis set with an effective core potential (ECP) for the lanthanum atom was chosen. A suitable basis set for the rare-earth atom was identified based on geometry optimizations of LaB_2O_4F. All-electron basis sets were employed for all boron [18] and oxygen [19] atoms. Out of these results of geometry optimizations of LaB_2O_4F, the well-tested ECP46MWB_GUESS [20, 21] basis set was chosen for the lanthanum atom. All calculations were performed with the PBESOL functional [22] for the correlation- and exchange-functional, and the SCF convergence for the energy was set to 10^{-12} Eh. The overall computation time for the calculations of harmonic vibrational frequencies of LaB_2O_4F took five weeks on a cluster with 12 Intel Xeon CPU X5670 2.93 GHz processors.

Results and Discussion

Crystal structure of LaB_2O_4F

The new rare-earth fluoride borate LaB_2O_4F crystallizes in the orthorhombic space group *Pbca* (no. 61)

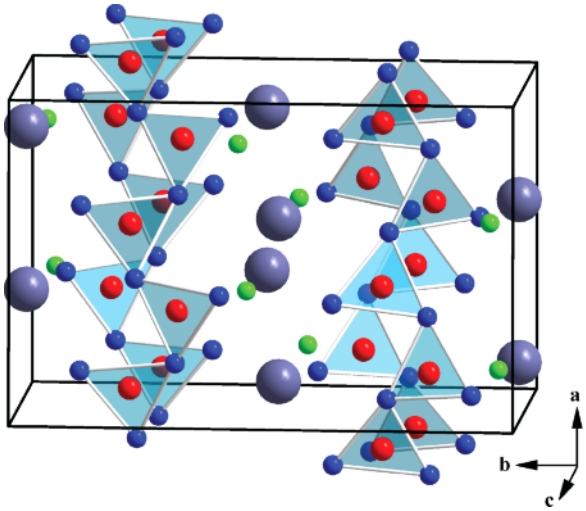

Fig. 2 (color online). Crystal structure of LaB_2O_4F (space group: *Pbca*), showing chains of linked BO_3 groups along *a*.

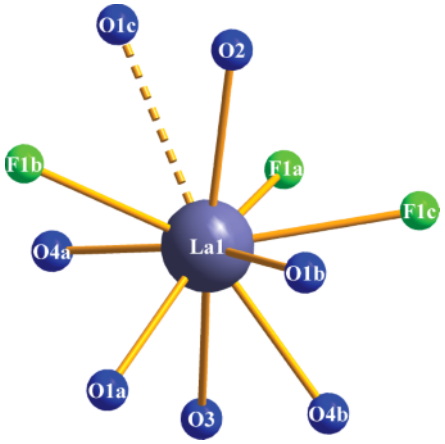

Fig. 3 (color online). The La^{3+} ion in LaB_2O_4F is surrounded by three fluoride and seven oxide anions.

with eight formula units per unit cell. The structure is composed of chains of corner-sharing triangular $[BO_3]^{3-}$ groups, 9+1 coordinated lanthanum cations, and threefold coordinated fluoride anions. Fig. 2 shows the crystal structure of LaB_2O_4F with its infinite chains of linked BO_3 groups along *a*. The structural motif of infinite chains of linked $[BO_3]^{3-}$ groups consists of two crystallographically different BO_3 groups (Δ), which can be described with the fundamental building block 1Δ:Δ (after Burns *et al.* [23]). In the structural chemistry of borates, this structural motif is relatively rare. Beside the isotypic compound CeB_2O_4F [6], only CaB_2O_4 [24, 25], SrB_2O_4 [26], and the alkali metal borate α-$LiBO_2$ [27–29] contain this fundamental building block. The linkage of the trigonal-planar $[BO_3]^{3-}$ groups to infinite chains occurs by the oxygen atoms O2 and O3. The boron-oxygen distances inside the BO_3 units are between 132.3(5) and 140.7(5) pm with a mean value of 137.0 pm for B1 and between 132.2(5) and 139.7(5) pm with a mean value of 136.9 pm for the atom B2. These values fit very well with the average boron-oxygen distance of 137 pm inside trigonal-planar $[BO_3]^{3-}$ groups [30–32]. The mean O–B–O angles of 120.0° and 119.9° for B1 and B2 have exactly the value expected for angles in trigonal-planar units. Fig. 3 displays the coordination sphere of the lanthanum cation in the structure of LaB_2O_4F, which is coordinated by seven oxygen and three fluoride atoms, forming a 9+1 coordination. The interatomic La–O/F distances are between 238.2(2) and 301.2(3) pm with a mean value of 261.0 pm. The fluoride anion is coordinated by three lanthanum cations with distances between 238.2(2) and 262.3(2) pm with a mean value of 254.0 pm. Tables 4 and 5 show the interatomic distances of LaB_2O_4F. For a detailed description of the structure, the reader is referred to the paper of the isotypic compound CeB_2O_4F [6]. In this work, we briefly compare the isotypic phases REB_2O_4F (*RE* = La, Ce) and the results of the DFT calculation.

The bond-valence sums of LaB_2O_4F were calculated from the crystal structure for all ions, using the bond-length/bond-strength concept (ΣV) [33, 34] and the CHARDI concept (*char*ge *di*stribution in solids, ΣQ) [35]. The results of these calculations are listed in Table 6 and correspond well with the expected values of the formal ionic charges.

Furthermore, the MAPLE values (*MA*delung *P*art of *L*attice *E*nergy) [36–38] of LaB_2O_4F were calculated to compare them with the MAPLE values received from the summation of the binary components La_2O_3 [39], LaF_3 [40], and the high-pressure modification B_2O_3-II [41]. The value of 28 549 kJ mol^{-1} was obtained in comparison to 28 451 kJ mol^{-1} (deviation = 0.3 %), starting from the binary oxides [$^1/_3$·La_2O_3 (14 234 kJ mol^{-1}) + $^1/_3$·LaF_3 (5306 kJ mol^{-1}) + B_2O_3-II (21 938 kJ mol^{-1})].

Due to their isotypy, there is no large difference in the structures of LaB_2O_4F and CeB_2O_4F. Table 7 compares the unit cells, the coordination numbers of the rare-earth metal ions, and the bond lengths. A closer

Table 6. Charge distribution in LaB_2O_4F (space group: *Pbca*), calculated with the bond-length/bond-strength ($\sum V$) and the Chardi ($\sum Q$) concept.

	La1	B1	B2	O1	O2	O3	O4	F1
$\sum V$	+3.06	+3.02	+3.03	−1.98	−2.12	−2.12	−2.03	−0.85
$\sum Q$	+2.98	+3.03	+2.99	−1.95	−1.97	−2.03	−2.01	−1.04

Table 7. Comparison of the isotypic structures $RE B_2O_4F$ (RE = La, Ce).

Empirical formula	LaB_2O_4F	CeB_2O_4F
Molar mass, g mol^{-1}	243.53	244.74
Unit cell dimensions		
a, Å	8.2493(9)	8.2163(5)
b, Å	12.6464(6)	12.5750(9)
c, Å	7.3301(5)	7.2671(6)
V, Å^3	764.7(2)	750.84(9)
Coordination number (CN)		
$RE1$ (RE = La, Ce)	10	10
av. RE1–O/F (RE = La, Ce) distance, pm	261.0	259.3
av. B–O distance in $[B(1)O_3]^{3-}$, pm	137.0	137.1
av. B–O distance in $[B(2)O_3]^{3-}$, pm	136.9	136.9

look at the lattice parameters *a, b,* and *c* reveals the typical rise due to the higher ionic radius of La^{3+}, which is based on the lanthanoide contraction. Due to the fact that the size difference is marginally, no greater deviances of the bond lengths and angles are observed.

Vibrational spectroscopy

The spectrum of the FTIR-ATR measurement of LaB_2O_4F is displayed in Fig. 4. The assignments of the vibrational modes are based on a comparison with the experimental data of borates containing trigonal $[BO_3]^{3-}$ groups [42 – 46] and on quantum-mechanical calculations. For borates in general, absorption bands at 1200 – 1450 cm^{-1} and between 600 and 800 cm^{-1} are expected for $[BO_3]^{3-}$ groups. In the FTIR spectrum of the new lanthanum fluoride borate, these modes are detected between 1100 and 1450 cm^{-1} and between 600 and 800 cm^{-1}. No OH bands could be detected in the range of 3000 to 3600 cm^{-1}.

In order to complete the spectroscopic characterization, Raman spectroscopic measurements were performed on single crystals of LaB_2O_4F. In Fig. 5, the Raman spectrum of LaB_2O_4F is displayed. Bands below 500 cm^{-1} can be interpreted by La–O/La–F bending and stretching modes as well as lattice vibrations. Modes above 1200 cm^{-1}, between 600 and 800, and at $\sim$ 500 cm^{-1} can be assigned to vibrations of the $[BO_3]^{3-}$ groups [47, 48].

In the case of LaB_2O_4F, one must consider that the trigonal-planar BO_3 units are linked to further boron-oxygen units, forming infinite chains. Hence, every motion inside of one boron-oxygen unit induces motions in the connected units. Nevertheless, quantum-

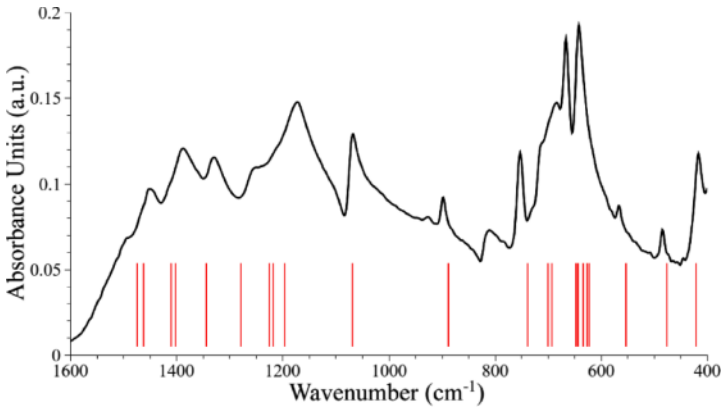

Fig. 4 (color online). FT-IR reflectance spectrum of a single crystal of LaB_2O_4F (black) and calculated vibrational bands (red lines).

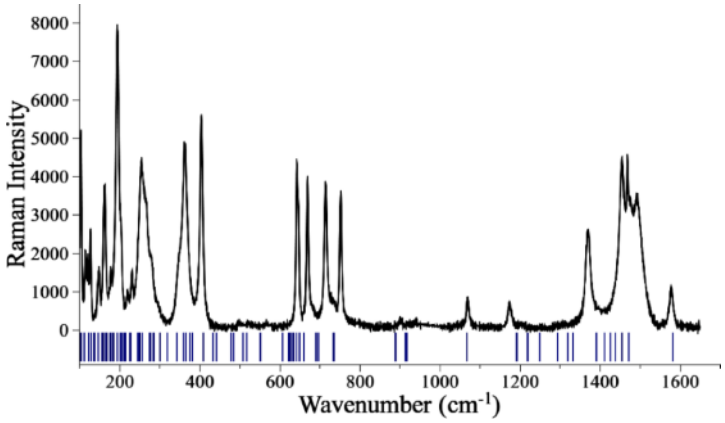

Fig. 5 (color online). Single-crystal Raman spectrum of LaB_2O_4F in the range of 100 – 1700 cm^{-1} (black) and calculated vibrational bands (blue lines).

chemical calculations of harmonic vibrational frequencies could be useful to assign vibrations of the excited groups.

Quantum-mechanical calculations of harmonic vibrational frequencies

To validate the quality of the basis sets and the functional, a geometry optimization of LaB_2O_4F was performed. Starting from the single-crystal structure, the geometry optimization yielded deviations less than one per cent for the lattice parameters and the atomic positions. The calculations of the harmonic vibrational frequencies were performed with the optimized geometry. The calculated bands fit well with the experimental spectra of LaB_2O_4F, especially the IR spectrum. The deviation results out of the approximations in the DFT method and the calculation of just one unit cell. Calculations of larger systems (supercells of LaB_2O_4F) were not possible. Moreover, the calculation did not consider the temperature (297 K for the experiment). Furthermore, the addition of two Gaussian peaks in the experimental spectrum led to a shift of the maxima. The large number of theoretical modes prevents a complete assignment of all vibrational modes. The intensities of the IR-active modes were calculated and the results are shown in Figs. 4 and 5.

The most intensive bands in the range of the experimental IR spectrum have been evaluated and compared with the experimental spectrum (Table 8). In the assignment, the highly condensed boron-oxygen framework must be considered. An exclusive stretching or bending motion inside a building unit is not possible. The evaluation of the IR bands shows that in the region of higher wavenumbers the excitation happened inside the trigonal $[BO_3]^{3-}$ groups as boron-oxygen stretching. As expected, the shortest boron-oxygen bonds have the bands at the highest wavenumbers (B2–O4 = 130.9(8) pm → 1473 cm^{-1} and B1–O1 132.4(9) pm → 1410 cm^{-1}). At 1068 cm^{-1} in the calculated spectrum and at 1060 cm^{-1} in the experimental spectrum, the B–O stretching mode of the longest boron-oxygen bond inside of the $[BO_3]^{3-}$ group is observed. Bands at lower wavenumbers become more and more dominated by bending modes. In the region 690 – 710 cm^{-1} (calculated at 692 cm^{-1}), the first

Table 8. Comparison and assignment of the most intensive theoretical and experimental IR bands in the spectrum of LaB_2O_4F.

Theoretical band	Experimental band or region	Assignment
1473	1450–1500	s(B2–O4)
1461	1450–1500	s(B2–O4)
1410	1390	s(B1–O1)
1401	1390	s(B1–O1)
1343	1325	s(B1–O3), s(B2–O3)
1278	1260	s(B1–O2)
1224	1200–1230	s(B2–O3)
1216	1200–1230	s(B2–O3)
1195	1185	s(O3–B1–O2)
1068	1060	s(B1–O2), s(B2–O2–B1)
887	890	b(B2–O3–B1)
738	750	b(B2–O2–B1)
699	690–710	b(B1–O3–B2)
692	690–710	b(B1–O3–B2), s(La1–O4), s(La1–F1)
476	480	b(O3–B2–O2)
420	410	b(La1–O4–La1),

s – stretching; b – bending; in brackets: pairs of bonded atoms with large relative motion between them.

lanthanum-oxygen and lanthanum-fluoride stretching modes are observed.

Out of the large number of theoretical Raman bands and the unavailability to calculate the intensity of the modes in the CRYSTAL09 programm, the assignments of the Raman bands are more difficult. The discrepancy between the theoretical and the measured bands indicates the difficulties in the theoretical prediction of Raman bands. As in the IR spectrum, the mode at the highest wavenumber (1583 cm^{-1}) corresponds to the shortest boron-oxygen bond (B2–O4 = 130.9(8) pm). Raman modes between 1400 – 1500 cm^{-1} can be assigned to boron-oxygen stretching modes. In the range of 650 – 800 cm^{-1}, bending modes b(B–O–B) are located. The strong band at about 400 cm^{-1} can be assigned to lanthanum-oxygen and lanthanum-fluoride stretching modes.

Conclusions

With the synthesis of LaB_2O_4F, the first compound isotypic to CeB_2O_4F has been discovered and characterized. In accordance with the relatively mild applied pressure of 1.1 GPa, the structure consists exclusively of trigonal-planar $[BO_3]^{3-}$ groups linked to infinite chains. These chains represent a rare type of fundamental building block in the chemistry of borates. The syntheses of the isotypic compounds in the series REB_2O_4F for smaller rare-earth cations like praseodymium or neodymium will be subject of our future efforts.

Acknowledgement

This research was funded by the Austrian Science Fund (FWF): P 23212-N19.

[1] H. Huppertz, *Chem. Commun.* **2011**, *47*, 131.
[2] G. Corbel, R. Retoux, M. Leblanc, *J. Solid State Chem.* **1998**, *139*, 52.
[3] E. Antic-Fidancev, G. Corbel, N. Mercier, M. Leblanc, *J. Solid State Chem.* **2002**, *153*, 270.
[4] H. Müller-Bunz, Th. Schleid, *Z. Anorg. Allg. Chem.* **2002**, *628*, 2750.
[5] A. Haberer, R. Kaindl, O. Oeckler, H. Huppertz, *J. Solid State Chem.* **2010**, *183*, 11970.
[6] E. Hinteregger, K. Wurst, M. Tribus, H. Huppertz, *J. Solid State Chem.* **2013**, *204*, 47.
[7] D. Walker, M. A. Carpenter, C. M. Hitch, *Am. Mineral.* **1990**, *75*, 1020.
[8] D. Walker, *Am. Mineral.* **1991**, *76*, 1092.
[9] H. Huppertz, *Z. Kristallogr.* **2004**, *219*, 330.
[10] D. C. Rubie, *Phase Transitions* **1999**, *68*, 431.
[11] N. Kawai, S. Endo, *Rev. Sci. Instrum.* **1970**, *41*, 1178.
[12] Z. Otwinowski, W. Minor in *Methods in Enzymology*, Vol. 276, *Macromolecular Crystallography*, Part A (Eds.: C. W. Carter Jr, R. M. Sweet), Academic Press, New York, **1997**, pp. 307.
[13] G. M. Sheldrick, SHELXS-97 and SHELXL-97, Program Suite for the Solution and Refinement of Crystal Structures, University of Göttingen, Göttingen (Germany), **1997**.
[14] G. M. Sheldrick, *Acta Crystallogr.* **2008**, *A46*, 112.
[15] R. Dovesi, V. R. Saunders, C. Roetti, R. Orlando, C. M. Zicovich-Wilson, E. Pascale, B. Civalleri, K. Doll, N. M. I. J. Bush, Ph. D'Arco, M. Llunell, CRYSTAL09, User's Manual, University of Torino, Torino (Italy), **2009**.
[16] R. Dovesi, R. Orlando, B. Civalleri, R. Roetti, V. R. Saunders, C. M. Zicovich-Wilson, *Z. Kristallogr.* **2005**, *220*, 571.
[17] F. Pascale, C. M. Zicovich-Wilson, F. Lopez, B. Civalleri, R. Orlando, R. Dovesi, *J. Comput. Chem.* **2004**, *25*, 888.
[18] R. Orlando, R. Dovesi, C. Roetti, *J. Phys.: Condens. Matter* **1990**, *38*, 7769.
[19] L. Valenzano, F. J. Torres, K. Doll, F. Pascale, C. M. Zicovich-Wilson, R. Dovesi, *Z. Phys. Chem.* **2006**, *220*, 893.
[20] M. Dolg, H. Stoll, A. Savin, *Theor. Chim. Acta* **1989**, *75*, 173.
[21] M. Dolg, H. Stoll, H. Preuss, *Theor. Chim. Acta* **1993**, *85*, 441.
[22] J. P. Perdew, A. Ruzsinszky, G. I. Csonka, O. A. Vydrov, G. E. Scuseria, L. A. Constantin, X. Zhou, K. Burke, *Phys. Rev. Lett.* **2008**, *100*, 136406.
[23] P. C. Burns, J. D. Grice, F. C. Hawthorne, *Can. Mineral.* **1995**, *3*, 1131.
[24] W. H. Zachariasen, *Proc. Natl. Acad. Sci. USA* **1931**, *17*, 617.
[25] M. Marezio, H. A. Plettinger, W. H. Zachariasen, *Acta Crystallogr.* **1963**, *16*, 390.
[26] J. B. Kim, K. S. Lee, I. H. Suh, J. H. Lee, J. R. Park, Y. H. Shin, *Acta Crystallogr.* **1996**, *C52*, 498.
[27] E. Höhne, L. Kutschabsky, *Z. Chem.* **1963**, *3*, 33.
[28] W. Zachariasen, *Acta Crystallogr.* **1964**, *17*, 749.
[29] A. Kirfel, G. Will, R. F. Stewart, *Acta Crystallogr.* **1983**, *B39*, 175.
[30] E. Zobetz, *Z. Kristallogr.* **1990**, *191*, 45.

[31] F. C. Hawthorne, P. C. Burns, J. D. Grice in *Boron: Mineralogy, Petrology and Geochemistry*, (Ed.: E. S. Grew), Mineralogical Society of America, Washington, **1996**.
[32] E. Zobetz, *Z. Kristallogr.* **1982**, *160*, 81.
[33] I. D. Brown, D. Altermatt, *Acta Crystallogr.* **1985**, *B41*, 244.
[34] N. E. Brese, M. O'Keeffe, *Acta Crystallogr.* **1991**, *B47*, 192.
[35] R. Hoppe, S. Voigt, H. Glaum, J. Kissel, H. P. Müller, K. J. Bernet, *J. Less-Common Met.* **1989**, *156*, 105.
[36] R. Hoppe, *Angew. Chem., Int. Ed. Engl.* **1966**, *5*, 95.
[37] R. Hoppe, *Angew. Chem., Int. Ed. Engl.* **1970**, *9*, 25.
[38] R. Hübenthal, MAPLE, Program for the Calculation of MAPLE Values (version 4), University of Gießen, Gießen (Germany), **1993**.
[39] N. Hirosaki, S. Ogata, C. Kocer, *J. Alloys. Compd.* **2003**, *351*, 21.
[40] E. Staritzky, L. B. Asprey, *Anal. Chem.* **1957**, *29*, 856.
[41] C. T. Prewitt, R. D. Shannon, *Acta Crystallogr.* **1968**, *B24*, 869.
[42] J. P. Laperches, P. Tarte, *Spectrochim. Acta* **1966**, *22*, 1201.
[43] H. Böhlhoff, U. Bambauer, W. Hoffmann, *Z. Kristallogr.* **1971**, *133*, 386.
[44] K. Machida, H. Hata, K. Okune, G. Adachi, J. Shiokawa, *J. Inorg. Nucl. Chem.* **1979**, *41*, 1425.
[45] A. Haberer, H. Huppertz, *J. Solid State Chem.* **2009**, *182*, 888.
[46] A. Haberer, M. Enders, R. Kaindl, H. Huppertz, *Z. Naturforsch.* **2010**, *65b*, 1213.
[47] A. Haberer, R. Kaindl, H. Huppertz, *Z. Naturforsch.* **2010**, *65b*, 1206.
[48] E. Hinteregger, G. Böhler, T. S. Hofer, H. Huppertz, *Z. Naturforsch.* **2013**, *68b*, 29.